Biochimica et Biophysica Acta 1808 (2011) 106–116

Contents lists available at ScienceDirect

Biochimica et Biophysica Acta

journal homepage: www.elsevier.com/locate/bbamem

Structure and mechanism of action of a *de novo* antimicrobial detergent-like peptide

Baptiste Legrand [a], Mathieu Laurencin [b], Joe Sarkis [a,d], Emilie Duval [c], Liza Mouret [a], Jean-François Hubert [a], Murielle Collen [a], Véronique Vié [d], Céline Zatylny-Gaudin [c], Joël Henry [c], Michèle Baudy-Floc'h [b], Arnaud Bondon [a,*]

[a] RMN-ILP, UMR CNRS 6026, PRISM, Université de Rennes 1, CS 34317, Campus de Villejean, 35043 Rennes Cedex, France
[b] ICMV, UMR CNRS 6226 Université de Rennes 1, 263 Avenue du Général Leclerc, 35042 Rennes Cedex, France
[c] UMR 100 IFREMER PE2M, Université de Caen Basse Normandie, 14032, Caen Cedex, France
[d] IPR, UMR CNRS 6251 Université de Rennes 1, 263 Avenue du Général Leclerc, 35042 Rennes Cedex, France

ARTICLE INFO

Article history:
Received 2 April 2010
Received in revised form 12 August 2010
Accepted 27 August 2010
Available online 15 September 2010

Keywords:
Antimicrobial peptide
Self-assembly
NMR
Circular dichroism
Detergent
Liposome

ABSTRACT

The K4 peptide (KKKKPLFGLFFGLF) was recently demonstrated to display good antimicrobial activities against various bacterial strains and thus represents a candidate for the treatment of multiple-drug resistant infections. In this study, we use various techniques to study K4 behaviour in different media: water, solutions of detergent micelles, phospholipid monolayers and suspension of phospholipid vesicles. First, self-assembly of the peptide in water is observed, leading to the formation of spherical objects around 10 nm in diameter. The addition of micelles induces partial peptide folding to an extent depending on the charge of the detergent headgroups. The NMR structure of the peptide in the presence of SDS displays a helical character of the hydrophobic moiety, whereas only partial folding is observed in DPC micelles. This peptide is able to destabilize the organization of monolayer membranes or bilayer liposomes composed of anionic lipids. When added on small unilamellar vesicles it generates larger objects attributed to mixed lipid–peptide vesicles and aggregated vesicles. The absence of calcein leakage from liposomes, when adding K4, underlines the original mechanism of this linear amphipathic peptide. Our results emphasize the importance of the electrostatic effect for K4 folding and lipid destabilization leading to the microorganisms' death with a high selectivity for the eukaryotic cells at the MIC. Interestingly, the micrographs obtained by electronic microscopy after addition of peptide on bacteria are also consistent with the formation of mixed lipid–peptide objects. Overall, this work supports a detergent-like mechanism for the antimicrobial activity of this peptide.

1. Introduction

Antimicrobial peptides (AMPs) are essential components of the host innate defence of wide array of organisms and show potential as new therapeutic agents against multi-resistant bacterial pathogens [1–5]. Databases report over 1000 sequences for natural AMPs (http://www.bbcm.univ.trieste.it or http://aps.unmc.edu/AP/main.php), while several thousand other sequences have been designed *de novo* and produced synthetically to enhance biological activities and bioavailability [6]. Although they differ widely in terms of sequence, AMPs usually consists of 12–50 residues, of which around 50% are hydrophobic and several cationic (to target negatively charged bacterial surfaces), having the potential to adopt an amphipathic secondary structure when bound to cell membranes. Many AMPs kill bacteria by permeabilization of the cytoplasmic membrane whereas others penetrate into the cell and target additional anionic intracytoplasmic constituents (e.g., DNA, RNA, proteins, or cell wall components) [7]. These modes of action require an interaction with the phospholipids within the cell membrane. The precise nature of AMP–membrane interactions remains controversial and actively debated. Numerous mechanisms have been proposed, including the barrel-stave pore [6], toroidal pore [8], aggregate [9], carpet-like [6] and detergent-like [10] models. All these models imply a first step corresponding to the interaction with the phospholipids of the membrane. This process has been shown to involve a highly dynamic association–dissociation mechanism for various peptides [11,12] inducing conformation changes of the bound peptides and possible self-association.

In a recent study, we described a particularly attractive *de novo* AMP that we called peptide K4 [13,14]. This 14 amino-acids peptide (KKKKPLFGLFFGLF) possesses a cationic polar head composed of four lysine residues and a lipophilic tail composed of ten hydrophobic residues. This linearly amphiphilic AMP exhibits a broad spectrum of antimicrobial activity on both Gram-positive and Gram-negative bacteria without hemolytic activity or cytotoxicity on eukaryotic cells at low minimum inhibitory concentration (MIC) levels. Moreover, we obtained images by scanning electron microscopy indicating that K4 kills bacteria by disrupting their cell membrane. We observed the

* Corresponding author. Tel.: +33 223236561; fax: +33 223234606.
E-mail address: arnaud.bondon@univ-rennes1.fr (A. Bondon).

0005-2736/$ – see front matter © 2010 Elsevier B.V. All rights reserved.
doi:10.1016/j.bbamem.2010.08.020

presence of numerous spherical elements in the medium with a diameter ranging from 0.2 μm to 0.7 μm. We proposed that these spheres correspond to microsomes composed of lipids from bacterial membranes after cell lyses by K4.

To test this hypothesis and get a better understanding of how this peptide destroys the pathogen agents, K4 was studied in various media, using different techniques: circular dichroism (CD), turbidity measurements, fluorescence spectroscopy, transmission electron microscopy (TEM), atomic force microscopy (AFM) and NMR. In water solution, K4 exhibits self-assembly at high concentration, producing nanostructures that could be observed on TEM. The critical aggregation concentration (*cac*) of K4 was determined by pulsed-field gradient spin-echo NMR (PGSE-NMR). Then, we used SDS detergent, phospholipid monolayers and phospholipid liposomes to study K4 behaviour in membrane-mimetic media. The peptide folding, when added to either detergent or liposomes, was followed by CD. NMR was used to determine the solution structure of K4 in the presence of SDS micelles. From NMR data as well as from turbidity measurements and calcein leakage experiments, we obtain evidence that, in the presence of K4, the anionic SUVs self-aggregate without disruption until they precipitate at high peptide/lipid ratio. Using anionic films, AFM images revealed fast adsorption of K4 in the monolayer leading to its destabilization.

We propose that K4 may act as a surfactant in building mixed microsomes composed of peptides and lipids. This destabilization mechanism of the bacterial membrane supports the "detergent-like model" previously described [10].

2. Materials and methods

2.1. Sample preparation

The K4 peptide was synthesized as described elsewhere [14]. Sodium-dodecyl-sulfate (SDS) and dodecyl-phosphocholine (DPC) were purchased from Sigma Aldrich. For NMR experiments, deuterated SDS-d25 (Euriso-top) was used. The phospholipid small unilamellar vesicles (SUVs) were prepared by sonication of a multilamellar vesicle (MLV) solution, as previously described [15]. The MLV solution was obtained by evaporation of phospholipids in chloroform and then rehydrating the film of lipids thus obtained with water. The neutral SUVs contain 1,2-dioleoyl-sn-glycero-3-phosphocholine (DOPC) whereas anionic SUVs were prepared using DOPC and 1,2-dioleoyl-sn-glycero-3-[phospho-L-serine] (DOPS) (Avanti Polar Lipids). The large unilamellar vesicles (LUVs) used in turbidity measurements and calcein leakage experiments were obtained by extrusion through 1 μm and 80 nm pore membranes, respectively (Avanti Polar lipids).

2.2. Circular dichroism

Circular dichroism (CD) experiments were carried out using a JASCO J-815 spectropolarimeter (Easton, USA) equipped with a Peltier device for temperature control. The spectra were obtained in water using a 2 mm path length CD cuvette, at 20 °C, over a wavelength range of 195–260 nm. Continuous scanning mode was used, with a response of 0.5 s with 0.1 nm steps, a bandwidth of 1 nm, and a scan speed of 50 nm per min. The signal to noise ratio was improved by acquiring each spectrum over an average of two to twenty scans depending on the K4 concentration. Spectra were recorded at pH 5, at several peptide concentrations in different environments: water, SDS solution, SUVs of DOPC and SUVs of DOPC:DOPS 2:1 solutions. Finally, each peptide spectrum was corrected by subtracting the background (either water, SDS, DPC or liposome spectrum) from the sample spectrum.

2.3. Transmission electron microscopy

The sample of 10 mM K4 peptide was deposited on Formvar coated grids, negatively stained with uranyl acetate and observed with a Jeol (JSM 1011) transmission electron microscope equipped with a megaview III camera (SIS) at the Microscopy Centre of the University of Caen (CMABio).

2.4. Turbidity measurement

The absorbance of phospholipid vesicle suspensions upon additions of K4 was measured at 350 nm on a Jasco V-650 spectrophotometer. SUVs were used as well as 1 μm diameter LUVs with total lipid concentration from 0.1 to 2.4 mM. The influence of anionic polar lipid headgroups on the interaction with K4 was studied using SUVs composed of different DOPC:DOPS ratios. In all experiments water was used as reference.

2.5. Calcein leakage experiments

Calcein was encapsulated into DOPC:DOPS 2:1 liposomes by dissolving a 125 mM MLV preparation in a 20 mM TRIS–HCl buffer (pH 7.5) containing 4 mM calcein (Sigma Aldrich) to a final lipid concentration of 10 mM. Liposomes were obtained by extrusion 30 times through 80 nm pore membranes. Untrapped calcein molecules were then removed by size-exclusion chromatography using a Sephadex G75 column with TRIS–HCl 20 mM as elution buffer. Fluorescence measurements were carried out on a SPEX 112 spectrofluorometer (Jobin-Yvon) at 20 °C. Excitation wavelength was set to 495 nm and emission spectra were recorded from 500 to 600 nm, exhibiting a maximum intensity at 515 nm. The emission fluorescence spectrum of the calcein-loaded vesicles was first recorded as a baseline. We used a 0.3 mM liposome preparation, which provides a convenient fluorescence intensity level. Total amount of calcein release was determined by adding 1.5 mM Triton X-100 to this solution, dissolving the lipid membrane without interfering with the fluorescence signal. Several additions of K4 peptide were carried out on 0.3 mM liposome preparations. Each experiment was three times reproduced.

2.6. Atomic force microscopy

A monolayer experimental system was used to experimentally observe the assembly behaviour of K4 peptide with lipid, and the transferred film was observed by AFM to investigate its structure on the air/water or lipid/water interface [16,17]. AFM imaging of Langmuir–Blodgett films (LB films) was performed in contact mode using a Pico-plus atomic force microscope (Agilent Technologies, Phoenix, AZ) under ambient conditions with a scanner of $10 \times 10\ \mu m^2$. Topographic images were acquired in constant force mode using silicon nitride tips on integral cantilevers with a nominal spring constant of 0.06 N/m. Samples for imaging were obtained using the Langmuir–Blodgett technique from Langmuir films.

2.6.1. Peptide on air/water interface

K4 solution was spread onto the interface, using a high-precision Hamilton microsyringe. The variation of surface pressure was measured using a Wilhelmy plate. After stabilization, the surface pressure was around 12 mN/m. The Langmuir film was transferred on freshly cleaved mica plates at constant surface pressure by raising (2 mm/min) the mica vertically through the air/water interface.

2.6.2. Peptide on lipid/water interface

A computer controlled system of user-programmable Langmuir troughs (Nima Technology, Cambridge, UK), equipped with two movable barriers, was used for the surface pressure measurements.

Lipid mixture of 1,2-palmitoyl-sn-glycero-3-phosphocholine (DPPC) and 1,2-palmitoyl-sn-glycero-3-phosphoglycerol (DPPG) (1:1 in chloroform/methanol) was gently deposited at the air/water interface of mQ water subphase. These saturated lipids were chosen because the DOPC:DOPS monolayer was unstable on the air/water interface. After 10 min to allow for evaporation of the solvent, lipid films of DPPC–DPPG lipid mixture were compressed by moving barriers at a rate of 8 cm^2/min and then equilibrated at the desired surface pressure of 29 mN/m. After stabilization, the K4 peptide was injected into the subphase using a microsyringe. The final concentration of the peptide in the trough was 60 μM. The surface pressure recording started at the same time as peptide injection into the subphase. The increase of surface pressure due to adsorption of the peptide onto the monolayer was recorded continuously as a function of time. The accuracy of surface pressure values was found to be better than 0.5 mN/m. After stabilization of the surface pressure (final surface pressure = 34.5 mN/m), the Langmuir film was transferred on freshly cleaved mica plates at constant surface pressure by raising (2 mm/min) the mica vertically through the lipid/water interface. Images were obtained from at least three samples prepared on different days with at least three macroscopically separated areas in each sample.

2.7. NMR spectroscopy

2.7.1. ^1H NMR

NMR samples for ^1H 1D spectra and 2D structural study spectra typically contain 1–2 mM K4 dissolved in H_2O:D_2O (90:10) or were prepared as micellar solutions containing 50 mM SDS d-25 (Eurisotop). To improve the signal visibility, the pH was adjusted to 5 and the temperature varied from 283 to 323 K, according to the media. Spectra were recorded on a Bruker Avance 500 spectrometer equipped with a 5 mm triple-resonance cryoprobe (^1H, ^{13}C and ^{15}N). Homonuclear 2D spectra DQF-COSY, TOCSY (MLEV) and NOESY were recorded in phase-sensitive mode using the States-TPPI method as data matrices consisting of 256–400 (t_1)×2048 (t_2) complex data points; 48 scans were carried out per t_1 increment with 1.5 s recovery delay and spectral width of 6009 Hz in both dimensions. The mixing times were 100 ms for the TOCSY; 100, 150 and 200 ms for the NOESY experiments. Spectra were processed with Topspin (Bruker Biospin) or the NMRpipe/NMRdraw [18] software package and visualized with Topspin or NMRview [19] on a Linux station. The matrices were zero-filled to 1024 (t_1)×2048 (t_2) points after apodization by shifted sine-square multiplication and linear prediction in the F1 domain. Chemical shifts were referenced with respect to the water chemical shift.

2.7.2. Paramagnetic relaxation enhancement experiments

Titration experiments were carried out by stepwise additions of $MnCl_2$ from 1 and 10 mM stock solutions in water on a NMR sample containing 1 mM K4 and 50 mM SDS at pH 5. The relaxation enhancements were monitored by recording 1D spectra after each addition of the Mn^{2+} paramagnetic cations (concentrations of 0.02, 0.035, 0.06, 0.075, 0.11, and 0.17 mM). Two-dimensional TOCSY experiments were also collected as 256 (t_1)×2048 (t_2) time-domain matrices over a spectral width of 4844 Hz, with 16 scans per t_1 increment and a mixing time of 80 ms.

2.7.3. ^{31}P NMR

^{31}P NMR spectra were recorded on a Bruker Avance 500 spectrometer equipped with a 5 mm BBO probe. A solution of 20 mM of DOPC:DOPS (2:1) SUVs in H_2O:D_2O (90:10), at pH 5 was used and spectra were recorded at 313 K for different K4 concentrations corresponding to 1/40 and 1/20 peptide to lipid ratios. At ratio 1/10, no phosphorus peak could be detected due to severe broadening.

2.7.4. Pulsed-field gradient spin-echo experiments

The pulsed-field gradient spin-echo NMR (PGSE-NMR) method [20,21] was used to measure the self-diffusion of K4 at different concentrations in H_2O:D_2O (90:10). Experiments were carried at 303 K and 323 K on the latter spectrometer. NMR signals give rise to exponential decays in the diffusion spectra, and the apparent translational diffusion coefficients were obtained with Topspin (Bruker Biospin) by fitting the following equation to the NMR data:

$$\ln\frac{I}{I_0} = -D\gamma^2 g^2 \delta^2 \left(\Delta - \frac{\delta}{3}\right) \quad (1)$$

with I and I_0 representing the measured and maximum intensities, respectively, D the translational diffusion coefficient, γ the ^1H gyromagnetic ratio, g the gradient strength, δ the pulsed-field gradient duration and Δ the diffusion delay time [22]. The gradient strength was varied from 0.007 to 0.32 Tm^{-1} in 16 steps, Δ was 50 ms in all experiments and values of 3.2 and 10 ms were used for δ when following respectively the water and the lipids signals, in this latter case water suppression with a watergate sequence was used. The K4 self-diffusion coefficients were obtained by calculating the mean values between coefficients measured from two groups of resonances, covering ^1H distributed along the whole peptide, the first group corresponding to the Leu6-Leu9-Leu13 CH_3 resonances and the second one to the four lysines εCH_2 and Phe7-Phe10-Phe11-Phe14 βCH_2 protons.

In addition, the translational diffusion coefficients of the anionic SUVs in the presence of increasing K4 concentrations were also determined. For this purpose, K4 was added on a solution of 12.5 mM DOPC:DOPS (2:1) SUVs in H_2O:D_2O (90:10), with the pH adjusted to 5 and at 298 K. K4 to lipid ratios 1/100 and 1/50 were used, giving rise to an increasing turbidity of the solution. Above the 1/20 ratio, lipid precipitation was observed. In all experiments the gradient strength was varied 0.007 to 0.32 Tm^{-1} in 16 steps. In order to follow the water and the lipids signals, Δ was set 50 and 100 ms, respectively, and δ was set to 3.2 and 20 ms, respectively. Again, to measure the lipids signals, a watergate sequence was used for water suppression. Data were treated as described previously to obtain the lipids self-diffusion coefficients through the analysis of the signals of the choline CH_3 headgroups, of the CH_2 acyl chains and of the CH_3 acyl chains.

2.8. Structure calculations

^1H chemical shifts were assigned according to classical procedures. NOE cross peaks were assigned and integrated within the NMRView software. Structure calculations were performed with the ARIA 2.2 software [23]. The calculations were initiated using the default parameters of ARIA and a set of manually assigned NOEs. The torsion angles φ were restrained to $-60\pm40°$ for $^3J_{HN\text{-}HA}$ lower than 6 Hz. At the end of each run, violations and proposed assignment by ARIA were checked before starting a new run. This process was repeated until all the NOEs were correctly assigned and no restraints were rejected. A last run of 100 structures was performed, in which the set comprising the 20 lowest energy structures without any distance restraint violation greater than 0.3 Å, was considered as representative of the peptide structure. Representation and quantitative analysis of the calculated structures were performed using MOLMOL [24] and PyMOL (Delano Scientific) softwares.

3. Results

The K4 peptide is studied here by using various technical approaches, in various media, namely pure water, water in the presence of neutral or negative micelles and water in the presence of lipidic monolayers or liposomes of different compositions. The data

are presented for each technical approach and the discussion is then divided in three parts: we first discuss the peptide self-assembling propensity, the structure obtained in micelles is then presented and the last part focuses on the peptide interactions with phospholipids.

3.1. Circular dichroism

CD spectroscopy was used to investigate the secondary structure of K4 in different media (Fig. 1). The CD spectrum of the peptide dissolved in water is characteristic of a random coil structure and no modification of the profile is observed upon addition of various salts up to 100 mM of NaCl, $NaHCO_3$ or Na_2HPO_4 (data not shown). By contrast, as shown in Fig. 1, the K4 structure is dependent on the SDS micelle concentration. In the presence of 3 mM SDS we can observe a weak negative band at 225 nm and a strong positive band around 201 nm. This shape is characteristic of a β-turn [25]. At higher concentration (50 mM SDS), K4 CD spectrum exhibits an α-helical trend, with minimal mean residue molar ellipticity values at 208 and 222 nm and a maximum close to 195 nm. In the presence of 50 mM DPC neutral micelles, the poorly defined spectrum displays a weaker α-helical character. The effect of SUVs addition is also sensitive to the charge of the phospholipids. When adding pure neutral DOPC SUVs, the CD spectrum remains characteristic of a random coil conformation as observed in water. In contrast, the addition of anionic SUVs composed of DOPC:DOPS mixture induces strong changes in the CD spectrum leading to a shape similar to that obtained by the addition of 3 mM SDS. Attempt to increase the SUV concentration was limited due to the strong absorption of phospholipids which imposes a maximum of 0.5 mM SUVs. At this concentration, a clear transition toward an α-helical profile cannot be observed.

3.2. Transmission electronic microscopy

Fig. 2 shows the micrograph of a water solution of K4 peptide at 10 mM. While few fibres can be observed, most of the peptide is present as spherical self-assembled structures with a mean diameter of around 10 nm.

3.3. Turbidity measurements

Absorbance measurements of several liposome suspensions were performed upon successive additions of K4, providing information on the vesicles behaviour as absorbance increase with the medium turbidity. First, the role of the anionic phospholipid in the K4 action on vesicles was studied using different liposome preparations. No absorbance increase is observed when adding K4 on neutral DOPC SUVs at 0.5 mM (Fig. 3A) and 1 mM (data not shown). This result demonstrates the weakness of the interaction of K4 with zwitterionic lipids. In contrast, addition of K4 on 0.5 mM SUVs made of several DOPC:DOPS ratios induces strong increases of the turbidity, as displayed in Fig. 3A. The extent of this increase is related both to the peptide concentration and the anionic phospholipid content. However, for each lipidic composition if enough peptide is added the solution becomes completely opaque and the absorbance saturates. This turbidity increase is attributed to vesicle aggregation induced by the peptide. At low K4 concentration the observed smooth turbidity increase can be attributed to an increase of the vesicle size due to peptide incorporation. The shapes of the curves, corresponding to the absorbance versus the peptide concentration, are strongly dependent on the DOPS content. At DOPS amounts of 10% and 20% of the total lipids, solutions turn abruptly opaque at very low K4 concentrations, 12.5 and 20 mM, respectively. The corresponding peptide to lipid ratio are 1/40 for 10% DOPS and 1/25 for 20% DOPS. But, for DOPS amounts

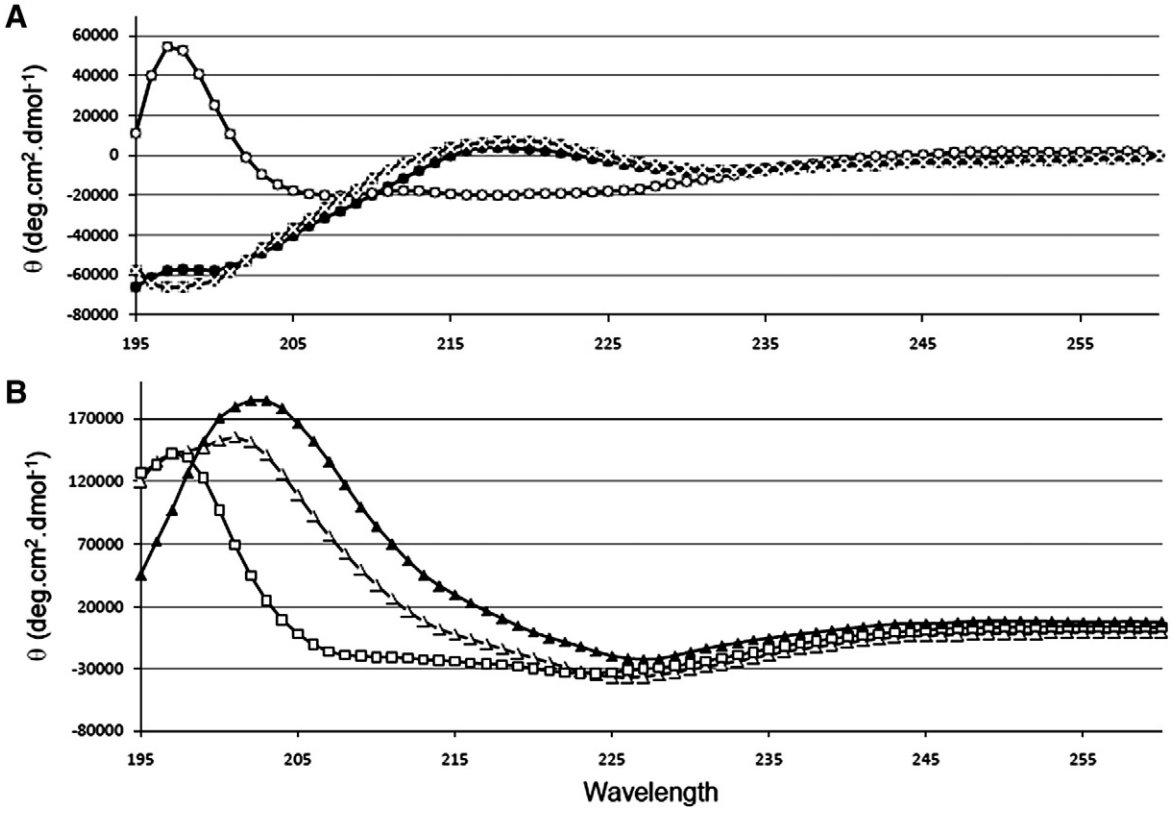

Fig. 1. 100 μM K4 peptide CD spectra in various media. (A) In water (open cross), in the presence of 0.5 mM neutral SUVs (black circles) and 50 mM DPC (open squares); (B) in the presence of 3 mM (open triangles) and 50 mM SDS (open squares) and 0.5 mM anionic SUVs (black triangles).

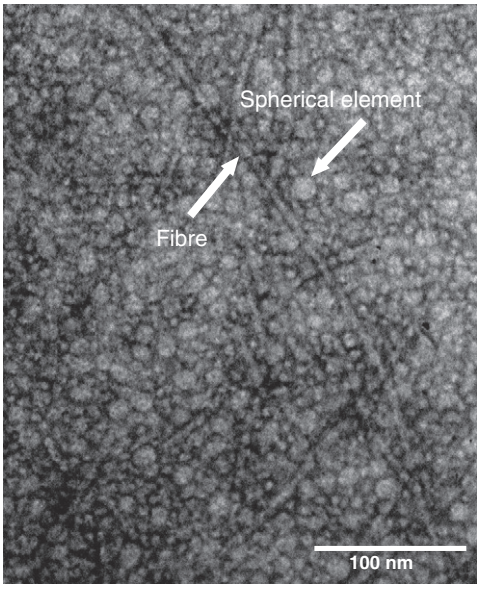

Fig. 2. Transmission electron micrograph of 10 mM K4 in water solution.

greater than 20% of total lipids, more K4 is needed for vesicle aggregation. Thus, anionic charges are required for the peptide to promote vesicle aggregation, but at high anionic phospholipid concentrations, electrostatic repulsion between vesicles probably interferes and competes with the peptide action. The high density of negative charges at the vesicle surface may also be responsible of the complete neutralisation of the K4 charges preventing aggregation.

Absorbance increase is also strongly related to the lipid concentration as shown in Fig. 3B, which displays the absorbance versus the peptide/lipid ratio. The experiment was performed using 0.5 mM DOPC:DOPS 70:30 SUVs. At this ratio, full absorbance saturation requires a peptide/lipid ratio of 0.09 (peptide at 45 μM) and good sensitivity versus the total lipid concentration is observed. Indeed for SUVs with a concentration of 2.4 mM aggregation is observed for a ratio around 0.015 (peptide at 35 μM) whereas lower SUV concentrations require a higher peptide/lipid ratio to start vesicle aggregation. This observation is consistent with a higher lipid concentration in favour of aggregation.

Experiments were also carried out on larger vesicles (LUVs of around 1 μm diameter) giving the same conclusion (data not shown). A progressive absorbance increase is observed upon K4 additions and aggregation occurs at lower peptide/lipid ratio for high lipid concentration.

Overall these experiments strongly emphasize the role of lipid polar heads in the interaction with K4. It is also consistent with a former step of incorporation of peptide in the lipid bilayers followed with an aggregative process.

3.4. Calcein leakage experiments

All fluorescence spectra were recorded for 0.3 mM liposome preparations. An emission fluorescence intensity of 1.3 ± 0.2 rfu (relative fluorescence units, arbitrary) was obtained at 515 nm for the quenched calcein entrapped into the vesicles. Total amount of calcein release obtained by Triton X-100 addition gave rise to an increase of fluorescence emission up to 2.62 ± 0.1 rfu, as the self-quenching was relieved. Several additions of the K4 peptide were successively performed to obtain 1/100, 1/50, 1/12 and 1/4 peptide to lipid ratios, but did not give rise to any significant increase in the fluorescence intensities (lower than 0.2 rfu in all experiments) showing no calcein leakage upon peptide addition. Thus, the K4 peptide destabilizes the vesicles without perforating the membrane,

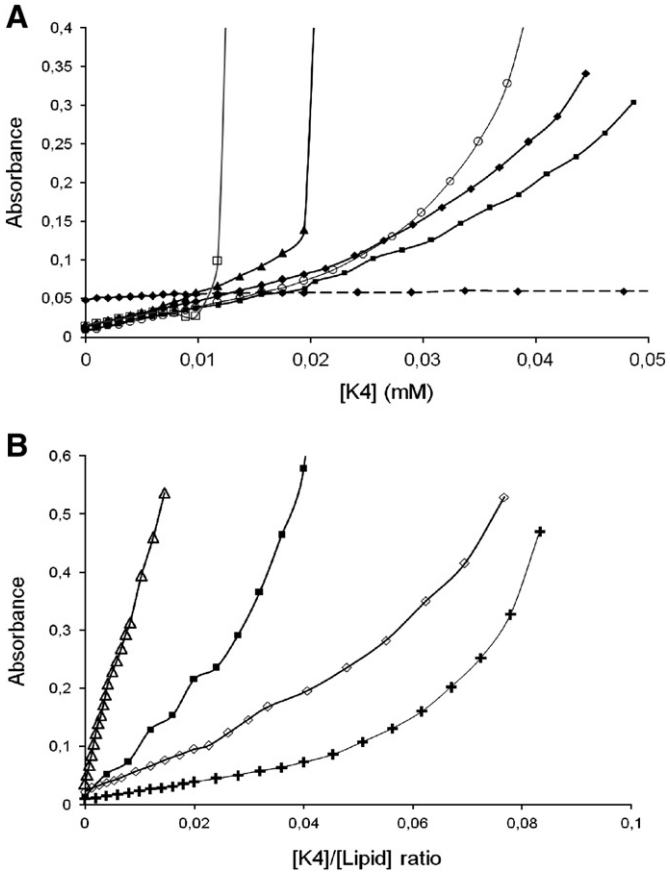

Fig. 3. Absorbance of liposome suspensions versus (A) K4 concentration or (B) peptide to lipid concentration ratios. For clarity, only the first steps of the absorbance increase are plotted. (A) DOPC SUVs at 0.5 mM (dashed line, black diamonds); DOPC:DOPS SUVs at 0.5 mM and 50:50 (black squares), 60:40 (black diamonds), 70:30 (open circles), 80:20 (open triangles) and 90:10 (open squares). (B) DOPC:DOPS 70:30 SUVs at 0.5 mM (cross symbols), 0.75 mM (open diamonds), 1 mM (black squares), and 2.4 mM (open triangles).

even at quite high concentrations. The absence of calcein leakage again points out that vesicle aggregation occurs upon peptide addition and suggests a specific mechanism of K4 which is not able to form pores in pure lipidic vesicles.

3.5. Atomic force microscopy

Atomic force microscopy was used to monitor the self-assembly of the peptide on the air–water interface, as well as the ordering of K4 with neutral (DPPC) and anionic lipid monolayer (DPPC:DPPG 80:20). The surface pressure of 29 mN/m was chosen from the literature as corresponding to a reasonable estimate of the surface pressure in biological membranes [26–29]. The data are presented in Fig. 4. On the air–water interface (Fig. 4A) the main information concerns the coarseness of the AFM image which is consistent with the presence of auto-assembled peptide structures. A few fibres can also be observed as previously encountered in the TEM micrograph. Such structures are also found in the AFM images obtained by allowing a K4 peptide solution to dry on mica surface (data not shown). When the peptide is injected under an anionic lipid monolayer (DPPC:DPPG), a high adsorption of the peptide to the monolayer can be observed through the increase of surface pressure recorded as a function of time (Fig. 1S, Supplementary data). With a high initial surface pressure ($\pi_i = 29$ mN/m), K4 penetrates easily into the monolayer and induces an increase of the surface pressure of 5.5 mN/m indicating that the peptide interacts with a high affinity for anionic membranes. AFM images (Fig. 4B–D) show a progressive

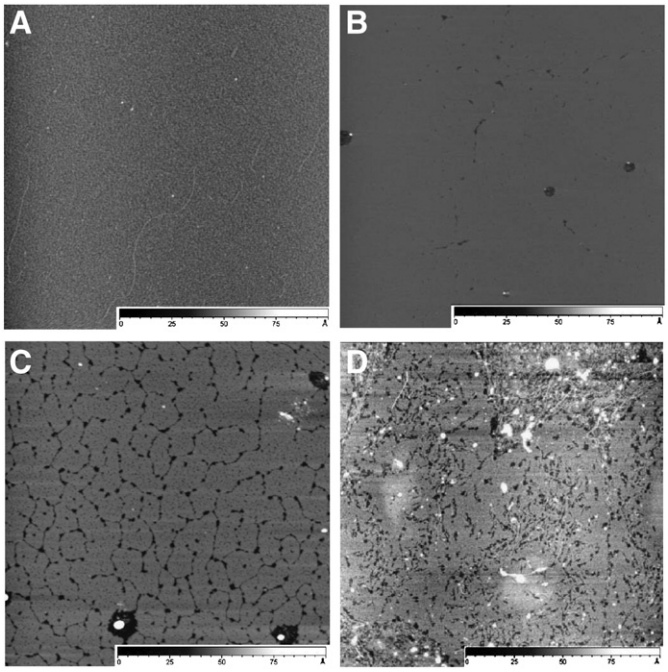

Fig. 4. AFM topographic images. (A) K4 peptide interfacial film transferred onto mica. (B) DPPC:DPPG (2:1) lipid monolayer at 29 mN/m. (C–D) Lipid/K4 monolayer at the end of adsorption of K4 at two different concentrations: (C) 60 μM and (D) 120 μM. For all images, scan size is $5\times5\ \mu m^2$, and height scale is 10 nm.

destabilization of the lipid monolayer after K4 injection into the subphase. The higher the concentration of K4 injected, the more the monolayer is destabilized. Using zwitterionic DPPC monolayers at the same initial surface pressure, the adsorption of K4 is found to be lower ($\Delta\pi = 3.5$ mN/m) than with previous anionic mixtures corresponding to a lower extent of penetration of the peptide (Fig. 2S, Supplementary data).

3.6. NMR spectroscopy and structure determination

We use proton 1D NMR to investigate the dependence of K4 structure on concentration in water, over a range of 2 to 20 mM (Fig. 5). Above 4 mM, we observe a severe broadening of all the peptide proton resonances. This broadening is associated with the ability of the K4 peptide to self-assemble at high concentration, while reversibility of the self-assembly is indicated by narrowing of the resonances obtained by dilution of the peptide. When looking in detail at the amide proton region, we note that this trend is more pronounced for the HN of residues localised in the hydrophobic tail. Hence, only the HN peaks of Lys3 and Lys4 are clearly observed for 20 mM K4 at 323 K. Further evidence for the self-assembly of K4 was obtained by measuring its diffusion coefficients (Fig. 6). The graphs exhibit a slope rupture around the concentration 5 mM. This behaviour appears to be quite similar as the one observed with surfactant molecules [30,31] and suggests a critical aggregation concentration (*cac*) above which the peptide is in a self-assembled form. Considering rapid exchange between free and self-assembled forms, the observed diffusion coefficient D is the mean value between that of free monomeric form D_{free} and aggregated form D_{agg}. This is usually described using the two-site exchange model [21].

$$D = \frac{C-cac}{C}D_{agg} + \left(1-\frac{C-cac}{C}\right)D_{free} \quad (2)$$

with C the peptide concentration. The data obtained above 6 mM were fitted to this equation giving *cac* values of 5.3 mM and 5.5 mM and

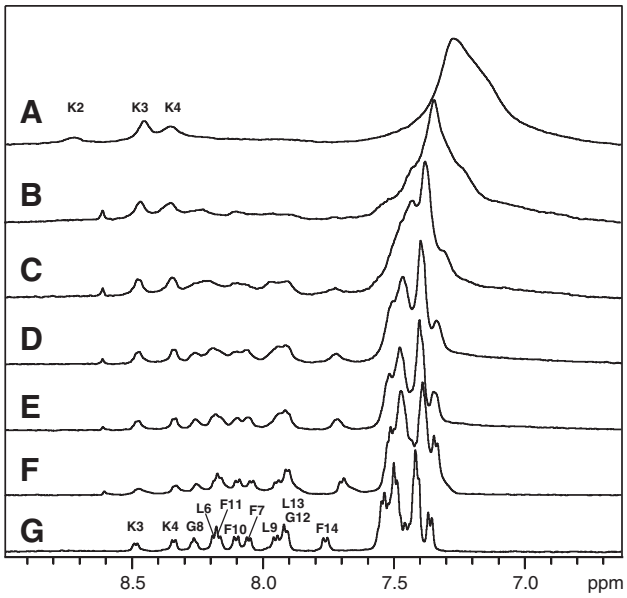

Fig. 5. Amide proton region of ^{1}H NMR spectra at 323 K, pH 5.0 (H_2O/D_2O) of K4 at various concentrations. (A) 20 mM, (B) 12 mM, (C) 10 mM, (D) 8 mM, (E) 6 mM, (F) 4 mM and (G) 2 mM.

D_{agg} values of $0.8\times10^{-10}\,m^2\,s^{-1}$ and $0.9\times10^{-10}\,m^2\,s^{-1}$ at respectively 303 K and 323 K.

Given the Stokes–Einstein equation

$$D = \frac{k_B T}{6\pi\eta r} \quad (3)$$

with D the diffusion coefficient of a particle, k_B the Boltzmann constant, T the temperature, η the viscosity and r the particle hydrodynamic radius, we then evaluated the aggregate size with

$$r_{agg} = r_{H_2O} \times \frac{D_{H_2O}}{D_{agg}} \quad (4)$$

with r_{agg} and r_{H_2O} the hydrodynamic radii of the self-assembled peptide and the water, respectively. The D_{H_2O} water diffusion coefficients at 303 K and 323 K were $2.89\times10^{-9}\,m^2\,s^{-1}$ and $4.57\times10^{-9}\,m^2\,s^{-1}$, respectively, and we used $r_{H_2O} = 0.11$ nm. These values combined with the previous D_{agg} ones gave diameters of 8 and

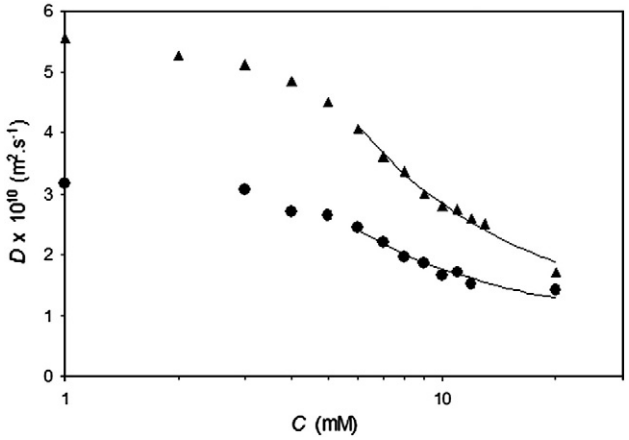

Fig. 6. Apparent diffusion translational coefficient (D) of the K4 peptide versus concentrations at 303 K (black circles) and 323 K (black diamond). Above 6 mM, the curves obtained by fitting Eq. (2) to experimental values are also shown (solid lines).

11 nm at 303 K and 323 K in good agreement with the TEM mean values of around 10 nm for the K4 self-assembled form.

1D spectra at a K4 concentration of 1 mM were recorded with increasing SDS concentrations (10, 20, 30, 50 and 200 mM, data not shown). No significant differences in terms of chemical shifts or line widths could be detected on the spectra with SDS at 50 and 200 mM. Thus the SDS concentration was set at 50 mM for the subsequent experiments corresponding to approximately 1.6:1 peptide to SDS micelle ratio assuming 60 SDS molecules by micelle [32]. The quality of the spectra is very good in water and SDS allowing us to assign nearly all the protons, despite the very close resonances of the methylene protons of the four lysines. The 2D spectra were acquired at 283 K in water, and at 293 K and 323 K in SDS detergent. The assignments, at 293 K and under the various studied conditions are presented in Tables 1S–3S in the Supplementary data.

In the presence of SDS micelles, most of the non-glycine residues in the hydrophobic tail, particularly Leu6, Phe7, Leu9, Phe10 and Phe11, exhibit $^{3}J_{HN\text{-}HA}$ coupling constants lower than 6 Hz. By contrast, in water, the amide proton $^{3}J_{HN\text{-}HA}$ coupling constants are all higher than 6 Hz. In agreement with the circular dichroism profiles, these results suggest that K4 does not adopt a characteristic structure in water, but is mainly helical in SDS detergent. The Pro5 appears to be in the *trans* conformation based on NOE patterns, since we can observe strong cross peaks between its H_δ and the H_α and H_β of the Lys4, as well as very weak NOE between the proline H_α and the preceding H_α and H_β protons.

For the ARIA final run, the K4 peptide structures in the presence of SDS, are calculated using 213 distance restraints and 5 dihedrals restraints (Table 4S, Supplementary data). The 20 lowest energy conformers, refined in a water shell, are represented in Fig. 7A. The global fold of the K4 peptide displays a well-ordered helical hydrophobic C-terminal moiety (6–14) and a disordered N-terminal region which contains the four lysines. The two parts are separated by the Pro5 residue which bends the peptide. Indeed, the backbone RMSD on the whole structure is 2.40 Å and falls to 0.86 Å if the poorly defined N-terminal moiety is ignored. Table 4S, Supplementary data, reports the RMSD values of backbone and heavy atoms on different regions of the peptide. On the helical wheel projection (Fig. 7B), we can see that the residues are distributed side by side according to their type. *i.e.* one side of the helix is composed of the four phenylalanines, a second of the three leucines and another with the two glycines. Without being typically amphipathic this residue distribution generates a "hydrophobic gradient" around the helix. The Pro5 residue bends and projects the polar N-terminal head outside the helix normal at the opposite side of the Leu moiety (Fig. 7). The peptide size in SDS micelles is about 2 nm which is less than half that of the extended conformation (about 5–6 nm) as shown in Fig. 7C.

No major structures were obtained neither in water nor in DPC micelles. Calculations with ARIA did not converge due to the small number and the low intensities of the NOE cross peaks.

The ^{31}P spectra of the DOPC:DOPS (2:1) SUVs were recorded after addition of peptide. As shown in Fig. 8, a pronounced broadening of the resonances is observed suggesting a gradual increase of the vesicle size induced by addition of the peptide. This was further reinforced by the self-diffusion coefficients measurements of the anionic SUVs in the presence of increasing K4 concentrations. The lipid diffusion coefficients decrease from $4.4\times10^{-11}\,m^2\,s^{-1}$, without K4, to $3.0\times10^{-11}\,m^2\,s^{-1}$ at the 1/100 peptide to lipid ratio and then $2.7\times10^{-11}\,m^2\,s^{-1}$ at the 1/50 ratio, suggesting vesicle size increase. Above the 1/20 ratio, lipid precipitation was observed. These values are mean ones between the coefficients measured from the choline CH_3 headgroups, the CH_2 acyl chains and the CH_3 acyl chains resonances.

4. Discussion

Antimicrobial peptides offer an interesting way of developing new antibiotic molecules. Numerous parameters modulate both

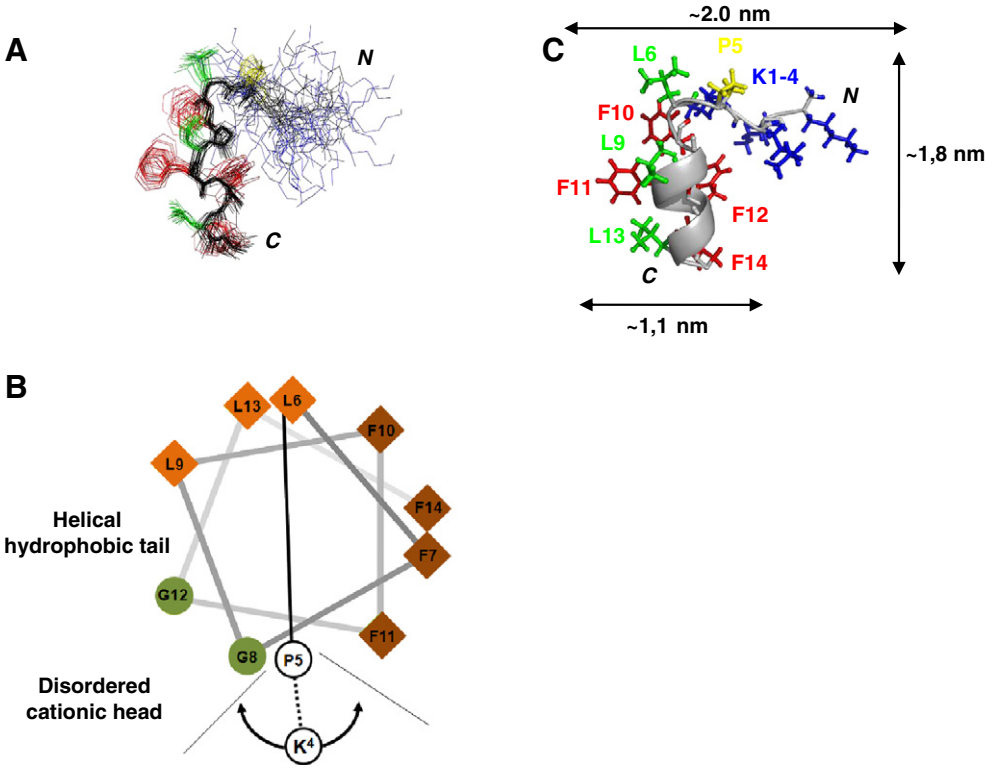

Fig. 7. Structures of K4 in the presence of 50 mM SDS micelles. (A) The 20 lowest energy structures of K4 derived from the 100 structures calculated in the final iteration of ARIA. The superposition was performed using the backbone atoms of residues 5–13. (B) Ribbon representation and sizes of the best structure of K4. The side chains are represented as stick (lysine in blue, proline in yellow, phenylalanine in red and leucine in green). (C) Helical wheel projection of the K4 peptide.

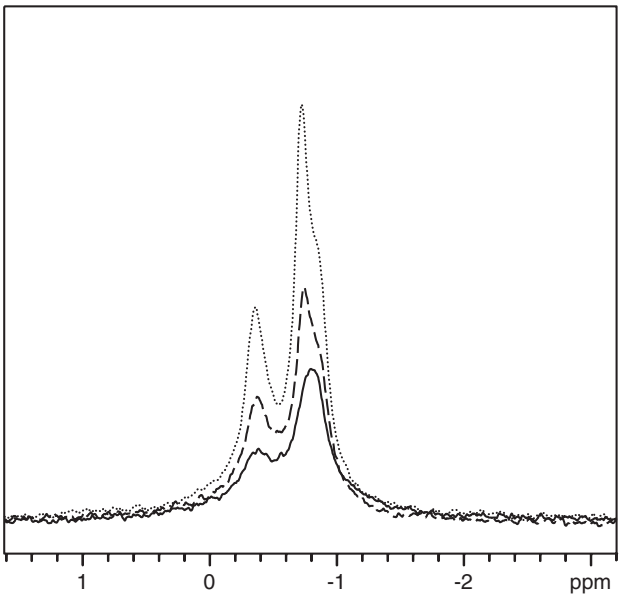

Fig. 8. ^{31}P NMR spectra of DOPC:DOPS (2:1) SUVs depending on the concentration of added K4 peptide: 20 mM SUVs alone (dotted line) and with a peptide/lipid ratio of 1:40 (dashed line) and 1:20 (continuous line).

antimicrobial and hemolytic activities including sequence, chain length, net positive charge, helical propensity, amphipathicity, hydrophobicity and hydrophobic moment [8,33–40]. Major improvements in the knowledge of the link between each of these variables and peptide activity allow us to the design *de novo* original active antimicrobial peptides. Thus, the peptide analysed in this study was constructed following several general rules using the Antimicrobial Peptide Database (APD: http://aps.unmc.edu/AP/main.html) [41]. The overall charge is cationic (+4), the C-terminal sequence is hydrophobic and comprises three leucine and four phenylalanine residues, and the hinge connecting the charged polar head and the hydrophobic segments is provided by a proline residue. This surfactant-like design is shown to be very efficient against several bacterial strains.

4.1. Self-assembling propensity

The K4 peptide is first studied in water by CD and NMR. At low concentration, no defined structure can be observed by CD, even in the presence of various salts which are able to induce a helical fold as encountered in the case of an amphipathic helix [42]. Proton NMR spectrum of K4 at low concentration is characteristic of the absence of any definite structure, whereas the increase of K4 concentration induces a severe broadening of all the peptide proton resonances in the NMR spectra. This broadening is associated with peptide aggregation; such an interpretation is further supported through the measurement of translational diffusion coefficients by pulsed-field gradient NMR experiments. We obtain a *cac* value of 5.3 mM at 303 K, while the estimated size of these auto-assembled objects is around 10 nm. In good agreement with the NMR data, we observe numerous spherical objects from 8 to 16 nm and few fibres on the TEM and AFM micrographs. K4 seems to promote the formation of micelles or vesicles. Unfortunately, the peptide concentration is too high to be studied by CD. Furthermore, NMR linewidths are too broad when the peptide is self-associated, preventing us from obtaining information on the K4 structure in this complex and on the self-assembly process. Based on the estimated size of the aggregate (10 nm), such large linewidths are consistent with slow dynamic behaviour between the monomeric and the aggregated peptide forms at the NMR chemical shift timescale. This slow dynamic is probably due to a strong packing between the hydrophobic side chains of the hydrophobic tail. This hypothesis is further supported by the observation that the self-assembly line-broadening is less pronounced for the four lysine linewidths of the peptide polar head, which are probably less compact due to charge repulsion and their exposure to the solvent. Nevertheless, dilution of the aggregate leads to a well-defined proton spectrum that is characteristic of the monomeric form of the peptide, thus demonstrating the reversibility of the self-association.

Self-assembling properties have already been encountered for small cationic surfactant-like peptides [43–49]. Indeed, the molecular and chemical similarities between the detergents or lipids and these peptides may explain their ability to self-associate in micelles, vesicles or in more complex nanostructures such as nanotubes. Nevertheless, to our knowledge, no data are available on the interaction of these nano-objects with the phospholipids.

4.2. Structural studies in micelles

Then, to investigate the peptide behaviour in a hydrophobic environment, we performed structural studies using CD and NMR spectroscopy in the presence of detergents. SDS and DPC micelles are very suitable as anionic and neutral membrane models in NMR studies because of the small size of the micelles and their high dynamic behaviour [50]. The CD spectrum of K4 in the presence of anionic SDS micelles, at high concentration, exhibits a helical trend, showing that this peptide adopts a well-defined structure in this hydrophobic environment whereas it remains unfolded in water. In agreement with the CD profile, the NMR structure of K4 is mainly helical in the presence of SDS. Indeed, as shown by structure calculations the hydrophobic tail is a well-defined helix (6–14) starting at the proline in position 5, with a disordered poly-lysine polar head. When using a paramagnetic probe, this poly-K cationic head strongly influences the interaction between the $MnCl_2$ and the peptide preventing the complete location of the peptide in the micelle. However, the hydrophobic tail along the micelle surface is consistent with the observed relaxation enhancement. This C-terminal moiety is composed of strongly hydrophobic residues (four Phe and three Leu) with a residue-dependent distribution (Fig. 7B). Most of helical cationic AMPs such as magainin, cecropin, mellitin etc are composed of amphipathic helices. Hence, the mechanism of K4 cannot be related to many other helical peptides, whether natural or synthetic, which display amphipathicity along their helix structure.

Interestingly, in DPC micelles, the K4 CD profile exhibits a weaker helical pattern and ARIA structure calculations do not converge. This highlights the fact that the K4 conformation is less stable in the presence of zwitterionic micelles and shows the role of the charge to induce the folding of the hydrophobic tail. The presence of the proline and two glycines affects the helix stability. This result could explain the high selectivity and low hemolytic activity of the K4 peptide considering that most microorganisms possess an anionic membrane in contrast to the external leaflet of eukaryotic cells, which are mainly composed of zwitterionic lipids. Generally, if no relation between the degree of helicity and antimicrobial activity is observed, high helicity is often related with high hemolytic activity [51]. Proline has been demonstrated to contribute to the short helical AMPs selectivity since the substitution of a single proline residue can decrease its antimicrobial activity and significantly increase its hemolytic activity [40].

4.3. Interaction with phospholipids

Peptide–lipid membrane interaction is a critical step in the mode of action of antimicrobial peptides and, whether as monomer or oligomers, it is widely believed that a non-specific binding process is

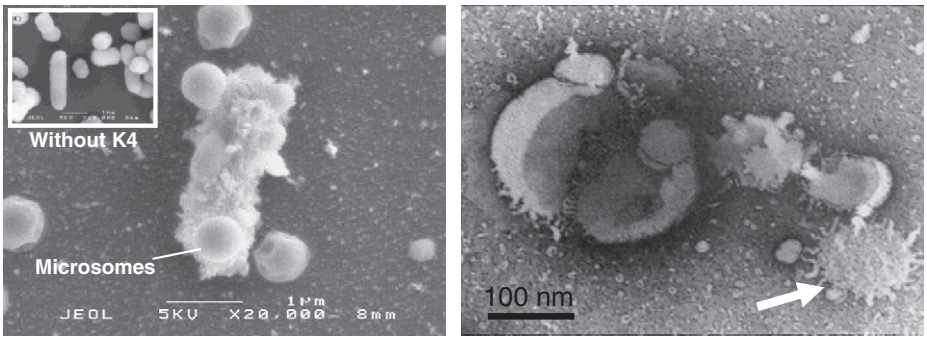

Fig. 9. Scanning electron micrographs of *E. coli* treated with K4. *E. coli* in mid-logarithmic growth was incubated with antibacterial peptide K4 for 2 h. Left: K4 was at a concentration of 100 μg/ml, and the inset corresponds to untreated bacteria (adapted from [14]). Right: Phosphocholine liposomes with SDS detergent adapted from [57].

responsible for peptide antimicrobial activity. Because of its short helical tail composed of 9 residues, K4 is not long enough to span the membrane bilayers, thus preventing pore formation.

To mimic the membrane, we used phospholipidic monolayers and SUVs or LUVs of different phospholipid compositions at different zwitterionic to anionic phospholipid ratios. The CD profile of the K4 peptide in the presence of neutral SUVs (DOPC) indicates a random coil as observed in water solution. Interestingly, K4 spectra in the presence of anionic SUVs (DOPC:DOPS 2:1) have a quite different shape, with a minimum at 228 nm, which is typical of a β-turn CD profile [25]. According to the previous results obtained with detergents, this observation highlights the role of the anionic hydrophobic environment into stabilizing a particular K4 conformation. Nevertheless, the CD profile does not exhibit a typical α-helical structure as obtained in the presence of SDS micelles but is similar to the intermediary β-turn spectra recorded in the presence of SDS at concentrations lower than the *cac*. As pointed out previously, due to signal broadening, we were unable to carry out a proton NMR structural study of K4 in the presence of SUVs. However, information about the SUV-peptide interaction can be extracted from 1D ^{31}P NMR spectra. Thus, the addition of K4 peptide onto SUVs of negatively charged phospholipids induces progressive increase of the vesicle size as highlighted by ^{31}P NMR line-broadening and translational self-diffusion coefficients measured by NMR. This phenomenon was also observed by turbidity experiments as addition of small K4 amounts on anionic vesicles induces absorbance increase. Such a progressive increase of the vesicle size has already been observed when adding detergent on liposomes [52–54]. At higher concentration, depending both on the total lipid concentration and the anionic polar head content, K4 induces anionic vesicle aggregation as observed by absorbance measurements. No absorbance increase was observed with zwitterionic vesicles suggesting the absence or a very weak interaction with K4. The association of the peptide with phospholipids and membrane destabilization is also consistent with the AFM data, demonstrating a destabilization of the anionic phospholipid monolayer.

It cannot be excluded that those favourable electrostatic interactions with anionic phospholipids could induce a local increase of the peptide concentration and subsequent peptide aggregate formation. However, such a process is not necessary to account for the bilayer destruction. It has been demonstrated with SDS micelles that lipid–detergent association occurs with the detergent in a monomer form suggesting that micelle formation is not a prerequisite for the formation of mixed lipid–detergent microsomes. This monomeric mode of action of detergent is observed even when detergent concentration is higher than the *cac* value [55,56]. In the present case, the K4 peptide is active on bacteria at concentration below its *cac* value and interaction with the membrane should occur in the monomeric state.

About the precise mechanism of K4 action, the calcein leakage experiments permit to conclude on the absence of pores induced by K4. In such a case, a mechanism involving a bactericidal site of action located inside bacteria could be proposed. However, scanning electron micrographs of *E. coli* treated with K4 displayed particles presumably composed of lipids and peptides (Fig. 9). Such a behaviour is also observed when adding SDS on liposomes (Fig. 9). In both cases apparent mixed lipid–peptide and lipid–detergent microsomes are formed. The difference in the sizes of the observed mixed microsomes can be related to the sizes of the precursors; K4 was added on full sized bacteria [14] whereas SDS was added on liposomes [57]. Obviously, the formation of mixed lipids/peptides objects requires the disruption of the bacterial membrane and is not in agreement with the observed absence of calcein leakage in the present study. The simplest way to explain this is to take into account of the difference between pure lipid liposomes and more complex cellular membrane of bacteria.

Among the different mechanisms of action of antimicrobial peptides, we propose that K4 is associated with the membrane and follows a detergent-like mode of action which involves a first step closely related to the carpet-like mechanism when the peptide is interacting as a monomer. We suggest that this leads to the formation of mixed peptide/lipid microsomes.

5. Conclusion

This study deals with K4 peptide behaviour in various media, with the aim of getting more information on the mode of action of this *de novo* antimicrobial peptide. In random coil conformation at low concentration in water, we demonstrate the self-assembly propensity of this peptide in water solution. By contrast, in the presence of SDS micelles, K4 adopts a well-defined partially helical structure, involving the hydrophobic moiety, comprising the residues 6 to 14. The interaction of K4 with liposomes is highly sensitive to the lipid polar heads. Partial folding of the peptide and membrane destabilization only occurs with the presence of negatively charged lipids. This suggests that electrostatic interactions play a major role in the initial recognition and membrane binding of the peptide. The localisation of the charge on one side of the peptide, with a hydrophobic tail in the other region confers an overall shape of K4 closely related with the one of detergent such as SDS. This analogy is also consistent with the self-assembly propensity of the peptide in water solution. Furthermore, when added on liposomes, K4 behaves like a detergent by increasing the vesicle size. Finally, a model involving the formation of mixed peptide/lipid microsomes is consistent with the SEM micrographs observed when K4 is added on bacteria. This study represents a valuable addition to our understanding of the mechanism of action of detergent-like AMPs which are able to destabilize the bacterial membranes.

Acknowledgements

We thank the Région Bretagne and SERB pharmaceutical company for financial support. We also thank the IFR 140 for providing support to the research platforms Spectroscopies and PRISM, as well as the IFR ICORE 146 for its support of the Electron Microscopy Center at the University of Caen (CMABio) and Didier Goux for Electron Microscopy experiments. M.S.N. Carpenter post-edited the English style.

Appendix A. Supplementary data

Supplementary data to this article can be found online at doi:10.1016/j.bbamem.2010.08.020.

References

[1] D. Andreu, L. Rivas, Animal antimicrobial peptides: an overview, Biopolymers 47 (1998) 415–433.
[2] S. Buchoux, J. Lai-Kee-Him, M. Garnier, P. Tsan, F. Besson, A. Brisson, E.J. Dufourc, Surfactin-triggered small vesicle formation of negatively charged membranes: a novel membrane-lysis mechanism, Biophys. J. 95 (2008) 3840–3849.
[3] R.M. Epand, H.J. Vogel, Diversity of antimicrobial peptides and their mechanisms of action, Biochim. Biophys. Acta 1462 (1999) 11–28.
[4] R.E. Hancock, D.S. Chapple, Peptide antibiotics, Antimicrob. Agents Chemother. 43 (1999) 1317–1323.
[5] M. Zasloff, Innate immunity, antimicrobial peptides, and protection of the oral cavity, Lancet 360 (2002) 1116–1117.
[6] Y. Shai, Mode of action of membrane active antimicrobial peptides, Biopolymers 66 (2002) 236–248.
[7] K.A. Brogden, Antimicrobial peptides: pore formers or metabolic inhibitors in bacteria? Nat. Rev. Microbiol. 3 (2005) 238–250.
[8] K. Matsuzaki, Y. Mitani, K.Y. Akada, O. Murase, S. Yoneyama, M. Zasloff, K. Miyajima, Mechanism of synergism between antimicrobial peptides magainin 2 and PGLa, Biochemistry 37 (1998) 15144–15153.
[9] M. Wu, E. Maier, R. Benz, R.E. Hancock, Mechanism of interaction of different classes of cationic antimicrobial peptides with planar bilayers and with the cytoplasmic membrane of *Escherichia coli*, Biochemistry 38 (1999) 7235–7242.
[10] B. Bechinger, K. Lohner, Detergent-like actions of linear amphipathic cationic antimicrobial peptides, Biochim. Biophys. Acta 1758 (2006) 1529–1539.
[11] P.F. Almeida, A. Pokorny, Mechanisms of antimicrobial, cytolytic, and cell-penetrating peptides: from kinetics to thermodynamics, Biochemistry 48 (2009) 8083–8093.
[12] M.T. Lee, W.C. Hung, F.Y. Chen, H.W. Huang, Mechanism and kinetics of pore formation in membranes by water-soluble amphipathic peptides, Proc. Natl. Acad. Sci. U. S. A. 105 (2008) 5087–5092.
[13] F.H.M. Baudy, G.C. Zatylnyj, J. Henry, E. Duval, M. Laurencin, Antimicrobial pseudopeptides, drug and pharmaceutical composition containing them, (Serb, Fr.; Centre National de la Recherche Scientifique Cnrs; Universite de Caen Basse Normandie), Application: FR, , 2009, 30 pp.
[14] E. Duval, C. Zatylny, M. Laurencin, M. Baudy-Floc'h, J. Henry, KKKKPLFGLFFGLF: a cationic peptide designed to exert antibacterial activity, Peptides 30 (2009) 1608–1612.
[15] G. Da Costa, S. Chevance, E. Le Rumeur, A. Bondon, Proton NMR detection of porphyrins and cytochrome c in small unilamellar vesicles: role of the dissociation kinetic constant, Biophys. J. 90 (2006) 55–57.
[16] M. Eeman, A. Berquand, Y.F. Dufrene, M. Paquot, S. Dufour, M. Deleu, Penetration of surfactin into phospholipid monolayers: nanoscale interfacial organization, Langmuir 22 (2006) 11337–11345.
[17] V. Vie, N. Van Mau, L. Chaloin, E. Lesniewska, C. Le Grimellec, F. Heitz, Detection of peptide–lipid interactions in mixed monolayers, using isotherms, atomic force microscopy, and Fourier transform infrared analyses, Biophys. J. 78 (2000) 846–856.
[18] F. Delaglio, S. Grzesiek, G.W. Vuister, G. Zhu, J. Pfeifer, A. Bax, NMRPipe: a multidimensional spectral processing system based on UNIX pipes, J. Biomol. NMR 6 (1995) 277–293.
[19] B.A. Johnson, R. Blevins, NMRVIEW: a computer program for the visualization and analysis of NMR data, J. Biomol. NMR 4 (1994) 603–614.
[20] M.D. Pelta, H. Barjat, G.A. Morris, A.L. Davis, S.J. Hammond, Pulse sequences for high-resolution diffusion-ordered spectroscopy (HR-DOSY), Magn. Reson. Chem. 36 (1998) 706–714.
[21] P. Stilbs, Fourier transform pulsed-gradient spin-echo studies of molecular diffusion, Prog. NMR Spectrosc. 19 (1987) 1–45.
[22] C.S. Johnson, Diffusion ordered nuclear magnetic resonance spectroscopy: principles, applications, Prog. NMR Spectrosc. (1999) 203–256.
[23] J.P. Linge, S.I. O'Donoghue, M. Nilges, Automated assignment of ambiguous nuclear overhauser effects with ARIA, Methods Enzymol. 339 (2001) 71–90.
[24] R. Koradi, M. Billeter, K. Wuthrich, MOLMOL: a program for display and analysis of macromolecular structures, J. Mol. Graph. 14 (1996) 51–55 29–32.
[25] M. Crisma, G.D. Fasman, H. Balaram, P. Balaram, Peptide models for beta-turns. A circular dichroism study, Int. J. Pept. Protein Res. 23 (1984) 411–419.
[26] A. Blume, A comparative study of the phase transitions of phospholipid bilayers and monolayers, Biochim. Biophys. Acta 557 (1979) 32–44.
[27] R.A. Demel, W.S. Geurts van Kessel, R.F. Zwaal, B. Roelofsen, L.L. van Deenen, Relation between various phospholipase actions on human red cell membranes and the interfacial phospholipid pressure in monolayers, Biochim. Biophys. Acta 406 (1975) 97–107.
[28] J.F. Nagle, Theory of lipid monolayer and bilayer phase transitions: effect of headgroup interactions, J. Membr. Biol. 27 (1976) 233–250.
[29] M.C. Phillips, R.M. Williams, D. Chapman, On the nature of hydrocarbon chain motions in lipid liquid crystals, Chem. Phys. Lipids 3 (1969) 234–244.
[30] V. Molinier, B. Fenet, J. Fitremann, A. Bouchu, Y. Queneau, PFGSE-NMR study of the self-diffusion of sucrose fatty acid monoesters in water, J. Colloid Interface Sci. 286 (2005) 360–368.
[31] L. Perez, A. Pinazo, M. Teresa Garcia, M. Lozano, A. Manresa, M. Angelet, M. Pilar Vinardell, M. Mitjans, R. Pons, M. Rosa Infante, Cationic surfactants from lysine: synthesis, micellization and biological evaluation, Eur. J. Med. Chem. 44 (2009) 1884–1892.
[32] S. Balayssac, F. Burlina, O. Convert, G. Bolbach, G. Chassaing, O. Lequin, Comparison of penetratin and other homeodomain-derived cell-penetrating peptides: interaction in a membrane-mimicking environment and cellular uptake efficiency, Biochemistry 45 (2006) 1408–1420.
[33] E. Glukhov, L.L. Burrows, C.M. Deber, Membrane interactions of designed cationic antimicrobial peptides: the two thresholds, Biopolymers 89 (2008) 360–371.
[34] E. Glukhov, M. Stark, L.L. Burrows, C.M. Deber, Basis for selectivity of cationic antimicrobial peptides for bacterial versus mammalian membranes, J. Biol. Chem. 280 (2005) 33960–33967.
[35] M. Dathe, J. Meyer, M. Beyermann, B. Maul, C. Hoischen, M. Bienert, General aspects of peptide selectivity towards lipid bilayers and cell membranes studied by variation of the structural parameters of amphipathic helical model peptides, Biochim. Biophys. Acta 1558 (2002) 171–186.
[36] M. Dathe, T. Wieprecht, Structural features of helical antimicrobial peptides: their potential to modulate activity on model membranes and biological cells, Biochim. Biophys. Acta 1462 (1999) 71–87.
[37] M. Dathe, T. Wieprecht, H. Nikolenko, L. Handel, W.L. Maloy, D.L. MacDonald, M. Beyermann, M. Bienert, Hydrophobicity, hydrophobic moment and angle subtended by charged residues modulate antibacterial and haemolytic activity of amphipathic helical peptides, FEBS Lett. 403 (1997) 208–212.
[38] P.M. Hwang, H.J. Vogel, Structure–function relationships of antimicrobial peptides, Biochem. Cell Biol. 76 (1998) 235–246.
[39] A. Tossi, C. Tarantino, D. Romeo, Design of synthetic antimicrobial peptides based on sequence analogy and amphipathicity, Eur. J. Biochem. 250 (1997) 549–558.
[40] S.T. Yang, J.Y. Lee, H.J. Kim, Y.J. Eu, S.Y. Shin, K.S. Hahm, J.I. Kim, Contribution of a central proline in model amphipathic alpha-helical peptides to self-association, interaction with phospholipids, and antimicrobial mode of action, FEBS J. 273 (2006) 4040–4054.
[41] Z. Wang, G. Wang, APD: the antimicrobial peptide database, Nucleic Acids Res. 32 (2004) 590–592.
[42] J. Johansson, G.H. Gudmundsson, M.E. Rottenberg, K.D. Berndt, B. Agerberth, Conformation-dependent antibacterial activity of the naturally occurring human peptide LL-37, J. Biol. Chem. 273 (1998) 3718–3724.
[43] S. Tsonchev, K.L. Niece, G.C. Schatz, M.A. Ratner, S.I. Stupp, Phase diagram for assembly of biologically-active peptide amphiphiles, J. Phys. Chem. B 112 (2008) 441–447.
[44] S. Vauthey, S. Santoso, H. Gong, N. Watson, S. Zhang, Molecular self-assembly of surfactant-like peptides to form nanotubes and nanovesicles, Proc. Natl. Acad. Sci. U. S. A. 99 (2002) 5355–5360.
[45] A.J. van Hell, C.I. Costa, F.M. Flesch, M. Sutter, W. Jiskoot, D.J. Crommelin, W.E. Hennink, E. Mastrobattista, Self-assembly of recombinant amphiphilic oligopeptides into vesicles, Biomacromolecules 8 (2007) 2753–2761.
[46] X. Yan, Y. Cui, Q. He, K. Wang, J. Li, W. Mu, B. Wang, Z.C. Ou-Yang, Reversible transitions between peptide nanotubes and vesicle-like structures including theoretical modeling studies, Chem. Eur. J. 14 (2008) 5974–5980.
[47] G. von Maltzahn, S. Vauthey, S. Santoso, S. Zhang, Positively charged surfactant-like peptides self-assemble into nanostructures, Langmuir 19 (2003) 4332–4337.
[48] R.V. Ulijn, A.M. Smith, Designing peptide based nanomaterials, Chem. Soc. Rev. 37 (2008) 664–675.
[49] H. Xu, J. Wang, S. Han, J. Wang, D. Yu, H. Zhang, D. Xia, X. Zhao, T.A. Waigh, J.R. Lu, Hydrophobic-region-induced transitions in self-assembled peptide nanostructures, Langmuir 25 (2009) 4115–4123.
[50] E. Strandberg, S.A. Ulrich, NMR methods for studying membrane-active antimicrobial peptides, Concepts Magn. Res. 23A (1994) 89–120.
[51] Z. Oren, Y. Shai, Selective lysis of bacteria but not mammalian cells by diastereomers of melittin: structure–function study, Biochemistry 36 (1997) 1826–1835.
[52] M. Cocera, O. Lopez, R. Pons, H. Amenitsch, A. de la Maza, Effect of the electrostatic charge on the mechanism inducing liposome solubilization: a kinetic study by synchrotron radiation SAXS, Langmuir 20 (2004) 3074–3079.
[53] M.A. Partearroyo, M.A. Urbaneja, F.M. Goñi, Effective detergent/lipid ratios in the solubilization of phosphatidylcholine vesicles by Triton X-100, FEBS Lett. 302 (1992) 138–140.

[54] U. Kragh-Hansen, M. le Maire, J.V. Moller, The mechanism of detergent solubilization of liposomes and protein-containing membranes, Biophys. J. 75 (1998) 2932–2946.
[55] M. Cocera, O. Lopez, J. Estelrich, J.L. Parra, A. de la Maza, Kinetic and structural aspects of the adsorption of sodium dodecyl sulfate on phosphatidylcholine liposomes, Langmuir 16 (2000) 4068–4071.
[56] M. Cocera, O. Lopez, J. Estelrich, J.L. Parra, A. de la Maza, Use of a fluorescence spectroscopy technique to study the adsorption of sodium dodecylsulfonate on liposomes, Chem. Phys. Lipids 109 (2001) 29–36.
[57] A. de la Maza, J.L. Parra, Vesicle–micelle structural transitions of phospholipid bilayers and sodium dodecyl sulfate, Langmuir 11 (1995) 2435–2441.